Articles

A Different Molecular Mechanism Underlying Antimicrobial and Hemolytic Actions of Temporins A and L

Alfonso Carotenuto,[§] Stefania Malfi,[§] Maria Rosaria Saviello,[§] Pietro Campiglia,[†] Isabel Gomez-Monterrey,[§] Maria Luisa Mangoni,[#] Ludovica Marcellini Hercolani Gaddi,[#] Ettore Novellino,[§] and Paolo Grieco*[,§]

Department of Pharmaceutical and Toxicological Chemistry, University of Naples "Federico II", I-80131 Naples, Italy, Department of Pharmaceutical Science, University of Salerno, I-84084 Fisciano, Salerno, Italy, and Department of Biochemical Science, Cenci Bolognetti Foundation—Pasteur Institute, "A. Rossi Fanelli", University of Rome "La Sapienza", I-00185 Rome, Italy

Received December 20, 2007

In this work, the naturally occurring antimicrobial peptides temporin A (TA) and L (TL) are studied by spectroscopic (CD and NMR) techniques and molecular dynamics simulation. We analyzed the interactions of TA and TL with sodium dodecyl sulfate (SDS) and dodecylphosphocholine (DPC) micelles, which mimic bacterial and mammalian membranes, respectively. In SDS, the peptides prefer a location at the micelle−water interface; in DPC, they prefer a location perpendicular to the micelle surface, with the N-terminus imbedded in the hydrophobic core. TL shows higher propensity, with respect to TA, in forming α-helical structures in both membrane mimetic systems and the highest propensity to penetrate the micelles. Hence, we have proposed a different molecular mechanism underlying the antimicrobial and hemolytic activities of the two peptides. We also designed new analogues of TA and TL and found interesting differences in their efficacy against microbial species and human erythrocytes.

Introduction

Gene-encoded antimicrobial peptides (AMPs) are considered key components of the innate immunity, which is found throughout the living world.[1–3] An ever increasing number of these molecules have been isolated from a vast array of biological sources, either prokaryotic or eukaryotic organisms, including humans, which they protect from the invasion of bacteria, protozoa, fungi, and viruses.[2,4,5] AMPs display an extreme diversity in their primary and secondary structures and usually have a rather large spectrum of antibiotic activity. As highlighted by Hans Boman,[6] the low selectivity and fast killing of microbes are crucial features of this peptide-based defense mechanism and make it as an "instant" immune system against microbial invaders. This immediate host response to infections plays an important role not only in invertebrates, which exclusively depend on it, but also in higher vertebrates, where it comes into action before the adaptive immunity is activated.[7,8] To face the challenge posed by the spreading resistance of pathogenic microorganisms to conventional drugs, the production of alternative antibiotics with new modes of action and resistance-avoiding properties has become an emergency. Among the possible candidates, AMPs are actually attractive molecules to be potentially developed as therapeutic anti-infective agents[2,9,10] and even as food preservatives.[11] Amphibian skin represents an incredibly rich source of AMPs, which are stored in granules of dermal glands and secreted upon stress or contact with microorganisms.[3,12] Among AMPs from amphibia, temporins are a family of related molecules, first isolated from the skin of the European red frog *Rana temporaria*.[13] Many other members of this group, counting now over 50 peptides, have later been found in several other *Rana* species and also in the venom of wasps.[14–17] Structurally, temporins are characterized by being short peptides (10–14 residues), with a net positive charge at neutral pH and a potential to adopt an amphipathic α-helix structure upon contact with membranes or in hydrophobic environments. Their consensus sequence is FLPLIASLLSKLL-NH_2.[16] Previously, temporins were found to be active particularly against Gram-positive bacteria, *Candida* species, fungi and with the ability to bind and permeate both artificial and biological membranes.[12,18–21] In this work, we focused on temporin A (TA) and temporin L (TL, Table 1) because of their different spectra of antimicrobial activity and toxicity. In particular, temporin A is preferentially active against Gram-positive bacteria,[14,19] including some clinically important antibiotic-resistant isolates,[14] displays a low lytic activity against human erythrocytes,[19] and kills efficiently the human parasitic protozoan *Leishmania*.[22] Differently, among all temporins studied to date, temporin L has the strongest activity against fungi, yeasts, Gram-positive and Gram-negative bacteria, erythrocytes, and cancer cells.[18,23]

Table 1. Sequences of Analyzed Peptides

peptide	sequence
TA	H-Phe[1]-Leu[2]-Pro[3]-Leu[4]-Ile[5]-Gly[6]-Arg[7]-Val[8]-Leu[9]-Ser[10]-Gly[11]-Ile[12]-Leu[13]-NH_2
TL	H-Phe[1]-Val[2]-Gln[3]-Trp[4]-Phe[5]-Ser[6]-Lys[7]-Phe[8]-Leu[9]-Gly[10]-Arg[11]-Ile[12]-Leu[13]-NH_2
Gln[3]-TA	H-Phe[1]-Leu[2]-Gln[3]-Leu[4]-Ile[5]-Gly[6]-Arg[7]-Val[8]-Leu[9]-Ser[10]-Gly[11]-Ile[12]-Leu[13]-NH_2
Pro[3]-TL	H-Phe[1]-Val[2]-Pro[3]-Trp[4]-Phe[5]-Ser[6]-Lys[7]-Phe[8]-Leu[9]-Gly[10]-Arg[11]-Ile[12]-Leu[13]-NH_2

It is widely accepted that the main target of AMPs is the lipid bilayer of the bacterial membrane instead of specific

* To whom correspondence should be addressed. Phone: +39-081-678620. Fax: +39-081-678644. E-mail: pagrieco@unina.it.
[§] University of Naples "Federico II".
[†] University of Salerno.
[#] University of Rome "La Sapienza".

10.1021/jm701604t CCC: $40.75
Published on Web 03/28/2008

membrane protein receptors.[24] It is supposed that differences in lipid composition between bacterial and mammalian cell membranes are the main reason for the selectivity of AMPs toward microbial cells.[24–26] However, numerous AMPs, like TL, can also bind and permeate the membrane of mammalian cells. Any attempt to design a peptide for therapeutic use would then be aided by a clear understanding of the structural elements that are responsible for its interaction with both mammalian and bacterial cell membranes. This would help in engineering new peptide sequences with similar/better antimicrobial activities but with a lower toxicity, assuming that these properties are distinct and separable in the primary structure of the peptide. The lipid composition of bacterial membranes is quite different from that of eukaryotic cells. Bacterial membranes include substantial amounts of negatively charged phospholipids such as phosphatidylglycerol and cardiolipin.[27] In contrast, the membrane of eukaryotic cells is composed mainly of phosphatidylcholine (PC), sphingomyelin, and cholesterol, all of which are neutrally charged at physiological pH.[28] To investigate how TA and TL interact with the phospholipid components of both bacterial and mammalian membranes, spectroscopic and computational methods have been used to study their interactions with sodium dodecyl sulfate (SDS) and dodecylphosphocholine (DPC) micelles,[a] which mimic bacterial and mammalian membranes, respectively.[29] Micelles possess a well-defined hydrophobic core and a flexible, hydrophilic interface like lipid bilayers. Indeed, micelles are commonly used in place of phospholipid monolayers or bilayers in methods such as NMR spectroscopy.[30,31] Although there is no direct correlation between the structure of the SDS headgroup and that of phospholipids composing a bacterial membrane, the SDS micelle is generally considered to be a good model for bacterial membranes because it possesses an anionic outer surface and a hydrophobic inner core.[32,33] In contrast, DPC micelles are considered as good models of eukaryotic cell membranes, which are generally rich in zwitterionic phospholipids. On the basis of spectroscopic results, we designed new analogues of TA and TL and found interesting differences in their efficacy against microbial species and human erythrocytes.

Results

Chemistry. Peptides were synthesized according to the solid phase approach using standard Fmoc methodology in a manual reaction vessel[34] (see Experimental Section).

The purification was achieved using a semipreparative RP-HPLC C-18 bonded silica column (Vydac 218TP1010). The purified peptides were 98% pure as determined by analytical RP-HPLC. The correct molecular weight of the peptide was confirmed by mass spectrometry. FAB-MS analyses were performed by MALDI.

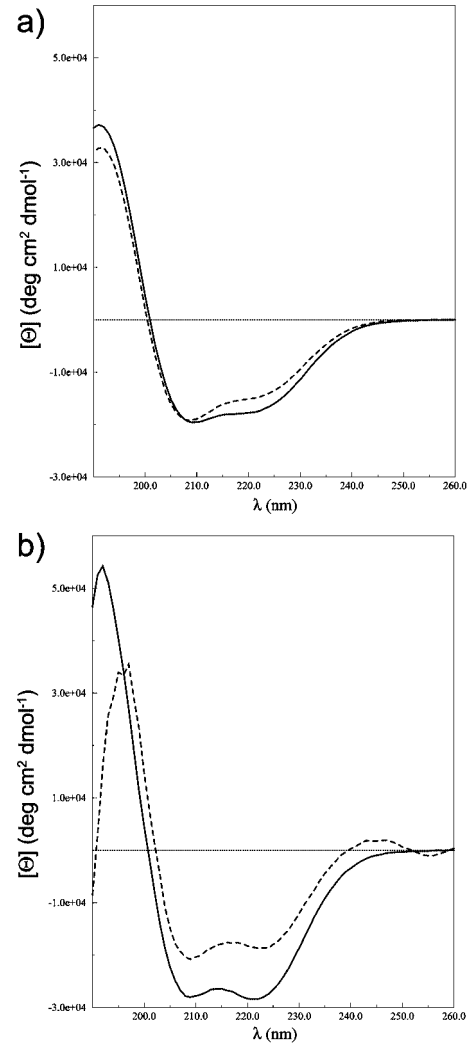

Figure 1. CD spectra of TA (a) and TL (b) in DPC (solid line) and SDS (dashed line) solutions.

CD Spectroscopy. To explore the conformational behavior of TA and TL, we first performed a CD study of these peptides in water, SDS/water, and DPC/water solutions (Figure 1). CD spectra in water (pH 7.4) suggest the presence of disordered conformers with a minimum close to 200 nm (data not shown). These results are in line with previous studies that indicated the absence of defined secondary structures for TA[14,19,35,36] and TL[35,37] in water solution. In contrast, in aqueous SDS and DPC micelles solution (20 mM) the shape of the CD spectra of TA and TL suggests the presence of α-helix folding with two minima around 209 and 222 nm. TA interactions with DPC and SDS were similar (Figure 1a). Relevant spectra show two minima around 209 and 222 nm indicative of helical structures. β-Structures are also evidenced, since the minimum at 209 nm is more intense (absolute minimum) compared to that at 222 nm. Comparing SDS and DPC solutions, we observe an increase in the helical content of the peptides in the latter case as the relative minimum at 222 nm becomes more intense. The conformational changes of TL induced upon its interaction with the zwitterionic DPC micelles were significantly more pronounced than those observed upon interaction with negatively charged SDS (Figure 1b), indicating that the α-helical content of TL in DPC is greater than that in SDS solution.

[a] Abbreviations: SDS, sodium dodecylsulphate; DPC, dodecylphosphocholine; SAR, structure–activity relationship; NMR, nuclear magnetic resonance; DQF-COSY, double quantum filtered correlated spectroscopy; TOCSY, total correlated spectroscopy; NOESY, nuclear Overhauser enhancement spectroscopy; NOE, nuclear Overhauser effect; MD, molecular dynamic; EM, energy minimization; 1D, 2D, and 3D, one-, two-, and three-dimensional; TSP, 3-(trimethylsilanyl)propionic acid; PC, phosphatidylcholine; SOPC, 1-stearoyl-2-oleoyl-*sn*-glycero-3-phosphocoline; POPG, 1-palmitoyl-2-oleoyl-*sn*-glycero-3-phosphoglycerol; DCM, dichloromethane; DIPEA, *N*,*N*-diisopropylethylamine; DMF, *N*,*N*-dimethylformamide; Et_3SiH, triethylsilane; Fmoc, 9-fluorenylmethoxycarbonyl; HOBt, *N*-hydroxybenzotriazole; HBTU, 2-(1*H*-benzotriazole-1-yl)-1,1,3,3-tetramethyluronium hexafluorophosphate; Pbf, 2,2,4,6,7-pentamethyldihydrobenzofuran-5-sulfonyl; RP-HPLC, reversed-phase high-performance liquid chromatography; MALDI, matrix-assisted laser desorption/ionization. Abbreviations used for amino acids and designation of peptides follow the rules of the IUPAC-IUB Commission of Biochemical Nomenclature in *J. Biol. Chem.* **1972**, *247*, 977–983. Amino acid symbols denote L-configuration unless indicated otherwise.

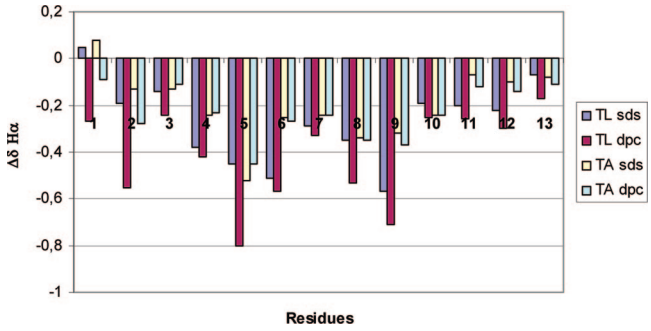

Figure 2. Plots of chemical shift deviations of H_α protons from random coil values. Random coil values were taken from ref 39b.

NMR Analysis. A whole set of 1D and 2D NMR spectra were collected for TA and TL. Spectra were obtained from aqueous solutions of both SDS and DPC (pH 4.5, $T = 298.1$ K). Complete ^{1}H NMR chemical shift assignments were effectively achieved for all the analyzed peptides according to the Wüthrich procedure[38] via the usual systematic application of DQF-COSY,[39] TOCSY,[40] and NOESY[41] experiments with the support of the XEASY software package (Supporting Information).[42] $^3J_{HN\text{-}H\alpha}$ couplings were difficult to measure probably because of a combination of smaller coupling constants (α-helical structure) and broader lines.

TL in SDS solution. Diagnostic NMR parameters observed for TL in SDS solution, H_α chemical shifts (Figure 2), NOE contacts (Figure 3), NH exchange rates, and temperature coefficients (Supporting Information), all indicate a conformational propensity toward helical structure. In particular, evidence for α-helix formation is provided by the analysis of the H_α resonances, which are strongly dependent on local secondary structure.[43]

Up-field shifts for H_α relative to random coil values are generally found for residues implicated in a α-helix or in turns and downfield shifts for those in β-sheets. As showed in Figure 2, H_α atoms from residue 2 to residue 13 experience upfield shifts of the NMR signals compared to those observed for the same amino acids in random coil state (Supporting Information). Additionally, a continuum stretch of NOE contacts of the types $d_{\alpha N}(i, i + 3)$ $d_{\beta\alpha}(i, i + 3)$ and $d_{NN}(i, i + 2)$ can be observed along the residues 3–12 (Figure 3a). Consistent with the CD results, all these data indicate the presence of a α-helix along the entire sequence of the peptide. The analysis of the exchange rates and of the temperature coefficients for the NH resonance indicated that such helical conformation is in equilibrium with more disordered conformations, since only NH resonances of residues 7, 10, and 11 show temperature coefficients ($-\Delta\delta/\Delta T < 3.0$ ppb/K) and exchange rates compatible with stable helical structures.

NMR-derived constraints obtained for TL in SDS were used as the input data for a simulated annealing structure calculation as implemented within the standard protocol of DYANA program.[44] NOE derived constraints were translated into interprotonic distances and used as upper limit constraints in subsequent annealing procedures to produce 200 conformations from which 100 structures were chosen, whose interprotonic distances best fitted NOE derived distances, and then refined through successive steps of restrained and unrestrained EM calculations using the program Discover (Biosym, San Diego, CA). An ensemble of 50 structures satisfying the NMR-derived constraints (violations smaller than 0.50 Å) was chosen for further analysis. As shown in Figure 4a, TL shows a α-helix structure encompassing residue 3–11 (rmsd = 0.5 Å for the backbone heavy atoms of these residues). The side chains orientation is also well defined (rmsd = 1.0 Å for the heavy atoms of residues 4–11). N- and C-terminal regions are less defined with the coexistence of folded and extended structures.

TL in DPC Solution. TL in DPC solution shows spectral features resembling those found in SDS solution. The differences between the NMR data in the two environments point to a higher conformational stability of TL in DPC micelle. In particular, we observed a higher number of medium range NOE connectivities (Figure 3b), longer NH exchange times, and lower temperature coefficients for almost all residues, indicating that these NH groups are engaged in stronger hydrogen bonds, stabilizing the helical structure (Supporting Information). Furthermore, H_α chemical shift values (Figure 2) are significantly upfield-shifted in DPC solution compared to SDS solution. The shift was mainly observed for residues 1, 2, and 5, which strongly indicates that the helical structure extends itself to the N-terminal residues in DPC solution. Other spectral features indicating the structure stabilization of the N-terminal portion of TL in DPC were (i) an intense downfield shift observed for Val^2 NH resonance (from 7.81 ppm in SDS to 9.23 ppm in DPC) and (ii) resonance degeneracy of Phe^1 H_β atoms observed in SDS (3.25 ppm) that was resolved in DPC solution (3.20 and 3.47 ppm).

NMR-derived constraints obtained for TL in DPC were used as the input data for a simulated annealing structure calculation as described above. For each peptide, 50 calculated structures satisfying the NMR-derived constraints (violations smaller than 0.35 Å) were chosen. As shown in Figure 4b, TL shows a α-helix structure encompassing all residues (rmsd = 0.3 Å for the backbone heavy atoms), with some conformational averaging only at the C-terminal ones. The side chain orientation is also well defined (rmsd = 0.7 Å for all the heavy atoms).

TA in SDS Solution. Diagnostic NMR parameters observed for TA in SDS solution indicate a conformational propensity toward helical structure. As shown in Figure 2, H_α atoms from residue 2 to residue 13 experience upfield shift of the NMR signals compared to those observed for the same amino acids in random coil state. Nevertheless, the analysis of the exchange rates and of the temperature coefficients for the NH resonance indicated that folded structures are in equilibrium with more disordered conformations, since only NH resonances of residues 7 and 11 show temperature coefficients ($-\Delta\delta/\Delta T < 3.0$ ppb/K) and exchange rates compatible with stable helical structures (Supporting Information). Furthermore, the simultaneous presence of $d_{\alpha N}(i, i + 2)$, together with some weak $d_{\alpha N}(i, i + 3)$ and $d_{\alpha N}(i, i + 4)$ dipolar couplings (Figure 3c), indicates the presence of β-turns in equilibrium with a α-helix structure, especially along the N-terminal fragment of the peptide.

Structure calculation (see above) gave an ensemble of 50 structures satisfying the NMR-derived constraints (violations smaller than 0.60 Å). All the structures of TA show a α-helix encompassing central residues 6–9 (Figure 4c). A few conformers (7/50) show the α-helix along almost the entire sequence (residues 3–12), while some (11/50) show a 3_{10}-helix along residues 10–12. Many structures (38/50) show the N-terminal residues in turn conformations. β-turns centered on Pro^3-Leu^4 and inverse γ-turns centered on Pro^3 could be observed.

TA in DPC Solution. TA in DPC solution shows spectral features resembling those found in SDS solution, with similar NOE connectivities (Figure 3d), NH exchange rates, NH temperature coefficients, and proton resonances (Supporting Information). The largest differences between the NMR data in the two environments are observed in the N-terminal region

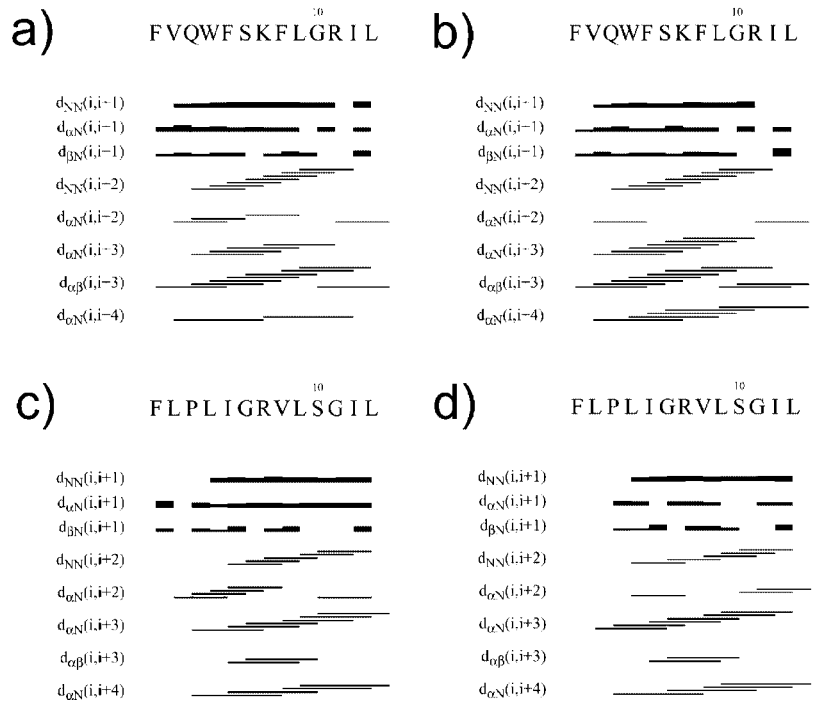

Figure 3. Schematic diagrams showing the NOE connectivities observed in the NOESY spectra of TL in SDS (a), TL in DPC (b), TA in SDS (c), and TA in DPC (d). Thickness of the bars is related to the NOE intensities.

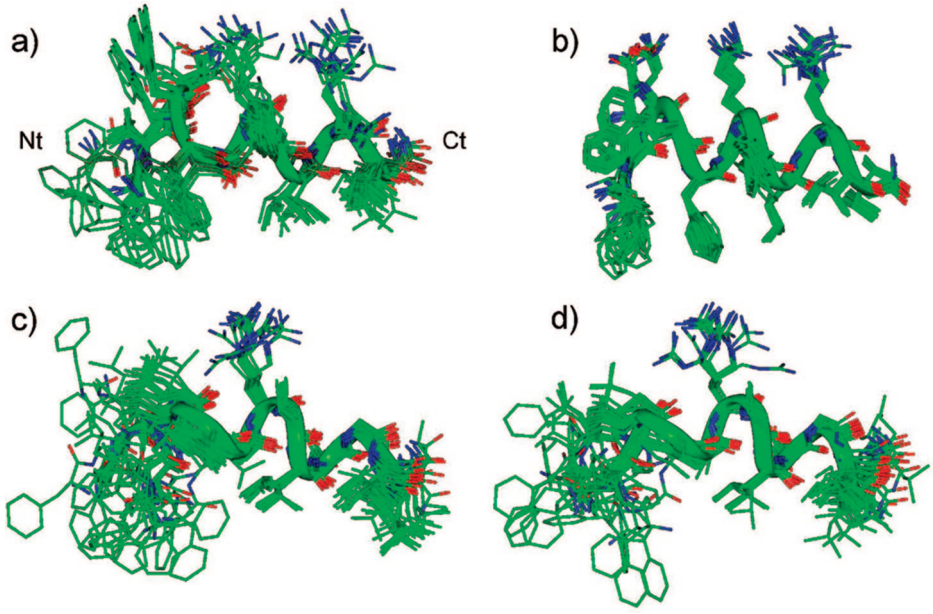

Figure 4. Superposition of the 20 lowest energy conformers of TL in SDS (a), TL in DPC (b), TA in SDS (c), and TA in DPC (d). Structures were superimposed using the backbone heavy atoms of residues 3–11. Heavy atoms are shown with different colors (carbon, green; nitrogen, blue; oxygen, red). Hydrogen atoms are not shown for clarity. Backbone atoms of the lowest energy conformer were evidenced as a ribbon: Nt, N-terminal; Ct, C-terminal.

of the peptide. In particular, H_α chemical shift values (Figure 2) for residues Phe[1] and Leu[2] are significantly upfield-shifted in DPC solution compared to SDS solution. Furthermore, significant shifts were observed for Leu[2] and Ile[5] NH resonances (from 8.10 ppm in SDS to 8.84 ppm in DPC for Leu[2]; from 7.50 ppm in SDS to 7.87 ppm in DPC for Ile[5]). Following structure calculation (see above) gave an ensemble of 50 structures satisfying the NMR-derived constraints (violations smaller than 0.50 Å). About half of the structures (24/50) folds in a α-helix structure along residues 3–12, and the other half-shows the β- and γ-turn structures about N-terminal residues observed in SDS (Figure 4d).

Topological Orientation. The positioning of the peptides TL and TA relative to the surface and interior of the SDS and DPC micelle was studied using paramagnetic probes: 16-doxylstearic acid and Mn^{2+}. Unpaired electrons lead to dramatically accelerated longitudinal and transverse relaxation rates of protons in spatial proximity via highly efficient spin and electron relaxation. Therefore, these paramagnetic probes are expected to cause broadening of the NMR signals and a decrease of

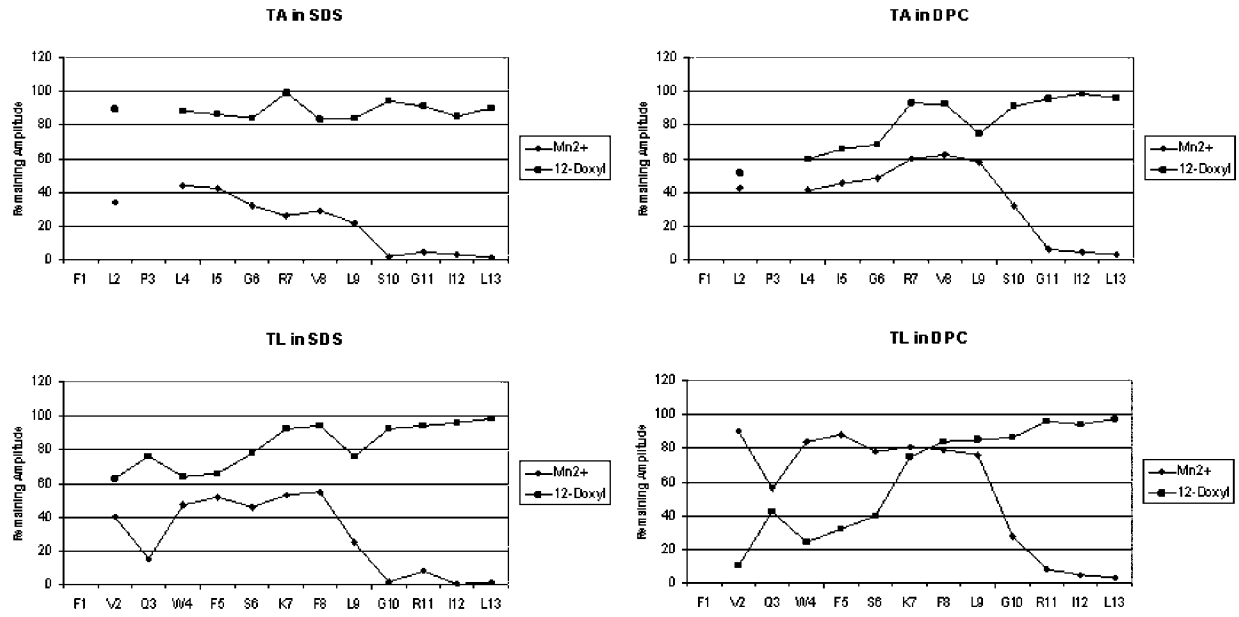

Figure 5. Remaining amplitude of NH/H_α TOCSY cross-peaks of TA (top panels) and TL (bottom panels) in 200 mM SDS (left panels) or DPC (right panels) after addition of paramagnetic probes.

resonance intensities from residues outside the micelle (Mn^{2+}) or deeply buried in the micelle (16-doxyl).[45] TOCSY spectra of TA or TL (in SDS or DPC solution) in the presence and in the absence of the spin labels, with all other conditions kept constant, were recorded (Figure 5).

Considering TA in SDS solution, all signal intensities remained almost constant after addition of 16-doxylstearic acid, thereby proving that no residues of TA in SDS become embedded in the hydrophobic core of the micelle. In the presence of Mn^{2+}, the ratios of volumes of all the NH/H_α were broadened and decreased in intensity, C-terminal residues being the most affected with a near-disappearance of the NH/H_α signals. Spin label results provide evidence that TA is located at the liquid−water interface of the SDS.

Concerning TA in DPC solution, the signal intensities of residues 2 and 4–6 showed significant reductions (about 30–40%) after the addition of 16-doxylstearic acid. Upon the addition of the Mn^{2+}, a generalized reduction of signal intensity was observed (>40% reduction) and more strongly for the C-terminal 11–13 residues (>90% reduction). These data can be explained admitting that an equilibrium takes place between a surface bound peptide and another state in which the N-terminus is inserted into the hydrophobic core of the micelle.

Considering TL in SDS solution, the signal intensities of residues 2, 4, and 5 showed reductions (about 30–40%) after the addition of 16-doxylstearic acid. Upon addition of Mn^{2+}, reduction of signal intensity was observed for all residues, mostly residue 3, and the C-terminal 10–13. Therefore, TL is preferentially located at the liquid−water interface of the SDS micelle. The reduction of the N-terminal residues signals upon addition of 16-doxylstearic acid indicates that the N-terminal tail of the peptide can flip inward and outward from the micelle core.

TL in DPC solution shows a reduction of intensity greater than 50% for N-terminal residues upon addition of 16-doxylstearic acid and a similar reduction for C-terminal residues upon the addition of Mn^{2+} (Figure 5). The data clearly indicate that the TL helix is placed perpendicularly to the micelle surface with its N-terminal region deeply buried within the micelle hydrophobic core and the C-terminal side outside, soaked in the water layer.

New Analogues. Design, Synthesis, and Biological Characterization. On the basis of the NMR and simulation results, we designed and synthesized new analogues of TL and TA (Table 1) with the aim of improving their pharmacological profiles. The antimicrobial activity of these peptides was evaluated as the ability to inhibit the growth of several Gram-positive, Gram-negative, and yeast species, using the microdilution broth method as reported in the Experimental Section. The results are shown in Table 2.

Pro^3-TL Analogue. Since the main difference observed between TA and TL secondary structures, both in SDS and DPC micelle solutions, was the presence of turn conformations in the N-terminal region of TA, likely induced by the Pro^3 residue, we investigated the role of this amino acid in both peptides. First, to obtain a TL analogue with a N-terminal turn structure, we replaced the Gln^3 with a Pro residue (Table 1).

The antimicrobial activity of this analogue was found to be equal to or 2-fold higher than that of the native peptide, against the yeast strains of *Candida albicans* and *Saccharomyces pombe*, the Gram-positive bacteria *Staphylococcus aureus* Cowan I and *Staphyloccocus epidermidis,* as indicated by the corresponding minimal inhibitory concentration (MIC) values, which were reduced by half (Table 2). Notably, the hemolytic activity on human erythrocytes was 2- to 5-fold lower than that of the natural TL, at a concentration range of 3–12 μM (Table 2).

Gln^3-TA Analogue. Analogously, we designed and synthesized a chimera derivative of TA in which Pro^3 was replaced by the Gln residue, which is present in the sequence of TL, at the same position (Table 1). It was supposed that this substitution should lead to a TA analogue with a higher propensity to the N-terminal helical structure.

With respect to the parent peptide TA, the hemolytic activity of Gln^3-TA became significantly stronger; in addition, a higher antimicrobial activity was detected against the Gram-positive strains *Bacillus megaterium*, *Staphylococcus aureus* ATCC 25923, *Staphylococcus epidermidis*, and *Streptococcus pyo-*

Table 2. Antimicrobial and Hemolytic Activities of Temporin analogues

	MIC (μM)[a]			
	TL	Pro^3-TL	TA	Gln^3-TA
Gram-negative bacteria				
Escherichia coli D21	12	12	>24	>24
Enterobacter faecalis ATCC 29212	6	6	12	6
Pseudomonas aeruginosa ATCC 15692	24	24	>24	>24
Pseudomonas syringae pv tobaci	6	6	>24	>24
Yersinia pseudotuberculosis YPIII	3	3	12	6
Gram-positive bacteria				
Bacillus megaterium Bm11	1.5	1.5	1.5	0.75
Staphylococcus aureus Cowan I	3	1.5	1.5	1.5
Staphylococcus aureus ATCC 25923	3	3	3	1.5
Staphylococcus capitis, 1	1.5	1.5	1.5	1.5
Staphylococcus epidermidis ATCC 12228	3	1.5	3	1.5
Streptococcus pyogenes ATCC 21547	6	6	12	6
Yeasts				
Candida albicans ATCC 10231	12	6	12	6
Saccharomyces cerevisiae	6	6	6	6
Saccharomyces pombe	6	3	3	3

	hemolysis			
peptide concn (μM)	TL	Pro^3-TL	TA	Gln^3-TA
3	13	6	3	9
6	48	10	4.5	18
12	92	42	6	70
24	94	92	28	92

[a] MW: TL 1640.02, Pro^3-TL 1609.01, TA 1396.80, Gln^3-TA 1427.81.

genes, the Gram-negatives *Y. pseudotuberculosis* and *Enterobacter faecalis*, and the yeast *Candida albicans* (Table 2).

Discussion

The purpose of this study is to provide a molecular resolution level of the interactions of TA and TL (Table 1) with the negatively charged SDS and zwitterionic DPC micelles (supposed to be a good model of bacterial and eukaryotic cell membranes, respectively) and to explain the different antimicrobial and hemolytic activities of these peptides, on the basis of their different interaction with the two types of micelles.

CD and NMR analyses revealed that both TA and TL adopt a random coil conformation in water solution and prefer a helical conformation in membrane mimetic environments (Figures 1−3). In both SDS and DPC solutions, the two analyzed peptides show structures that can be described as amphipathic α-helices at least when considering the central residues 6–9 (Figure 4). This result is in accordance with previous NMR studies with TA, using TFE (trifluoroethanol) solutions as rough mimic of hydrophobic environments.[14] Helical propensity of TA[14,19,35,36] and TL[35] was also assessed by CD spectroscopic analysis in TFE solutions. CD analysis of TA in SDS solution[36] and of TL in the presence of small unilamellar vesicles composed of SOPC (1-stearoyl-2-oleoyl-*sn*-glycero-3-phosphocoline) and POPG (1-palmitoyl-2-oleoyl-*sn*-glycero-3-phosphoglycerol)[37] also gave similar results.

In our studies, subtle differences could be observed in the conformational preferences of the two peptides in the different membrane mimetic environments. Helical character of TL significantly increases passing from SDS to DPC micelles. The whole peptide sequence is interested in this helical strengthening, but it is particularly evident at the N-terminal end of the peptide. In fact, residues Phe^1 and Val^2 changed from a disordered state to a helical conformation. In agreement with our result, Rinaldi et al. found that the membrane-permeabilizing ability of TL was greatest with liposomes consisting of the zwitterionic PC and that an increase in POPG content negatively influenced this activity.[18]

TA conformational behavior observed in SDS and DPC solutions was similar. Slight differences are localized in the N-terminal region of the peptide. In fact, mainly β- and γ-turn structures are observed in SDS micelle while an increased content of helical structures can be described in DPC.

Although a direct comparison of the conformational stability between TA and TL is not easy to make, overall spectroscopic data indicate that the propensity in forming α-helical structures is the following: TL in DPC solution > TL in SDS solution ≥ TA in DPC solution > TA in SDS solution. In line with our result, D'Abramo et al. demonstrated the higher stability of α-helix conformations in TL compared to TA.[35] Throughout an essential dynamics (ED) analysis approach of a 290 ns molecular dynamic (MD) simulation, they could conclude that both TA and TL (in water at 300 K) do not show any α-helix conformation, even though TL shows a higher propensity to form stable α-helices in water compared to TA. The authors also defined a core group of residues triggering the folding of both TA and TL, i.e., residues from 7 to 10. This region roughly overlaps with the most stable α-helical region obtained by our NMR analysis (residues 6–9).

The location of temporins with respect to the micelle depends on the peptide sequence and on the nature of the polar heads of the micelles. Our analysis with paramagnetic probes (Figure 5) showed that TA is located at the lipid−water interface, parallel to the membrane, when it interacts with negatively charged SDS micelle. In contrast, TL adopts a topological orientation perpendicular to the membrane when bound to the zwitterionic DPC micelle, with the N-terminus located close to the center of the micelle. Less defined pictures can be drawn when we consider the location of TA in DPC micelle and TL in SDS micelle. In those cases, the peptides are preferentially located at the liquid−water interface of the micelles, but they can occasionally flip inward the micelle core; an equilibrium of orientational states (inserted and surface-associated) may exist. The ability of the analyzed temporins to penetrate the micelles can be sorted as follows: TL in DPC solution > TA in DPC solution > TL in SDS solution > TA in SDS solution. Our result about TL localization in zwitterionic micelles agrees with that found by Zhao et al.[21,37] Using fluorescence spectroscopy, these authors showed that TL inserts deeply into the membrane in a perpendicular orientation and enhances the acyl chain order of the lipids. In another investigation, on the basis of the EPR (electron paramagnetic resonance) experiments on nitroxide-labeled fatty acids incorporated into PC liposomes,[20] TA was shown to lie parallel to the membrane surface.

Following our results, a different molecular mechanism underlying antimicrobial and hemolytic activities of TA and TL can be hypothesized. TA shows antimicrobial activity (preferentially against Gram-positive bacterial strains) and displays only minor hemolytic activity. It interacts with the SDS micelle, a bacterial membrane mimic, folding in α-helix conformation along its central residues (6–9), adopting turn conformations at the N-terminus and a more flexible conformation at the C-terminus. Further, the peptide localizes parallel to the water−membrane interface. A similar behavior was found for TL in SDS micelles, with only two minor differences: (i) the N-terminus of TL has a higher propensity to form helical structures; (ii) TL shows some tendency to flip inward the micelle core. The above snapshot about the temporins−SDS

micelles interaction could address to the "carpet-like" mechanism to explain the bacterial membrane disruption.[46] According to the "carpet model", peptides bind the phospholipid membrane surface until a threshold concentration is reached and then permeate it in a detergent-like manner.

The "dynamic peptide−lipid supramolecular pore" model has been proposed to describe the antimicrobial activity of temporins.[20] Briefly, according to this model,[25,47,48] AMPs bind to the outer leaflet of model membranes and flip inward, carrying the polar heads of the lipids with them. When a local high concentration of a peptide is reached, transient aqueous pores of variable sizes are formed. No detergent-like effect was observed, in the case of temporins, at the maximal peptide/lipid molar ratio tested (1:10).[20] However, we cannot exclude the possibility that at higher peptide/lipid ratios, major membrane disruption may occur, as suggested by the carpet model.[46] In our opinion, the two models (i.e."carpet" and "dynamic peptide−lipid supramolecular pore") are not in conflict with each other because the peptides can first form transient pores (as indicated in ref 20) that can increase in size when the peptide/lipid ratio increases. When the peptide/lipid ratio is very high (a situation not studied in ref 20), this could lead to membrane micellization.

In contrast, the highly hemolytic TL interacts with the DPC micelles, a mammalian membrane mimic, folding in α-helix conformation along the entire peptide sequence. TL localization is perpendicular to the DPC micelle surface, with the N-terminus located within the hydrophobic core. A "barrel-stave" model to explain hemolytic activity of TL can be invoked.[46] In this model, the peptides are supposed to form the staves of a barrel-like channel; the number of peptides that come together to form a channel will determine its size, whereas the stability of the barrel will determine the pore lifetime. Since peptide channels would require a minimum peptide length of ∼23 residues to span the membrane, it would be intriguing to determine the pore architecture of temporins. These peptides might form holes in a more elaborate way, perhaps involving their dimerization.[13,14] The low lytic activity of TA against human erythrocytes[13] could be explained considering its partial ability to insert within DPC micelles.

It is well-known that hydrophobic interactions play a major role in the activity of AMPs with bilayers made of zwitterionic phospholipids.[49] Since TA has higher hydrophobicity (H) and hydrophobic moment (μ) than TL ($H = 0.2246$ vs 0.06461, $\mu = 0.360$ vs 0.312),[20,21] it should better permeabilize the zwitterionic membrane, in contrast with the experimental results. We believe that this apparent contradiction can be explained by considering the slightly different conformational propensities of the two peptides. The main difference between the secondary structures of TA and TL was the presence of turn conformations in the N-terminal region of TA instead of the α-helix observed in TL. The loss of a regular helical conformation could explain the reduced ability of TA in penetrating DPC micelles. As a proof of the concept, we synthesized and evaluated the antimicrobial−hemolytic activities of a few rationally designed analogues. Since the turn structures are likely induced by the Pro^3 residue, we investigated the role of this position both in TA and in TL. With the aim of inducing a turn structure in a TL derivative, we replaced the Gln^3 of TL with a Pro residue (Table 1). Biological data of Pro^3-TL showed an increase of antimicrobial activity toward Gram-positive and yeast cells, with a decreased hemolytic activity with respect to the native TL (Table 2). Conversely, we designed and synthesized a chimera derivative of TA in which Pro^3 was replaced by the Gln residue, which occupies the same position in TL, obtaining the Gln^3-TA analogue. It had higher ability to lyse human red blood cells than the native TA, with an improved antimicrobial activity especially against Gram-positive bacterial strains and *Candida* (Table 2). A detailed conformational analysis of the new designed analogues is currently in progress. Conformation−activity relationships of the natural peptides TA and TL and the results obtained with the new analogues demonstrated that while the N-terminal helical structure is not required for the peptide ability to permeate the negatively charged membranes of bacterial cells, it appears to be a crucial structural element for binding and insertion into zwitterionic membranes and for hemolytic activity. A similar result was also found for a cell-selective diastereomer of melittin by Anglister et al.[50]

Conclusions

CD and NMR spectroscopies were used to determine the conformation and location of TL and TA in both zwitterionic DPC micelles, supposed to be a good model of eukaryotic cell membranes, and SDS micelles, a suitable mimic for the negatively charged bacterial membranes. Our results point to a different molecular mechanism underlying antimicrobial and hemolytic actions of TA and TL. In particular, the "dynamic peptide−lipid supramolecular pore" and the "barrel-stave" models were employed to interpret the antimicrobial and hemolytic activities of temporins, respectively. Biological activity of new rationally designed analogues confirms our hypothesis. In particular, with respect to the native TL, the analogue Pro^3-TL has shown an increased antimicrobial potency and a decreased hemolytic activity that make it an interesting molecule for further structure–function relationship studies.

Experimental Section

Synthesis. N^{α}-Fmoc-protected amino acids, HBTU, HOBt, and Rink amide resin were purchased from GL Biochem Ltd. (Shanghai, China). Peptide synthesis solvents, reagents, and CH_3CN for HPLC were reagent grade and were acquired from commercial sources and used without further purification unless otherwise noted. The syntheses of TL and TA analogues were performed in a stepwise fashion via the solid-phase method. N^{α}-Fmoc-Leu-OH was coupled to Rink amide resin (0.5 g, 0.7 mmol NH_2/g). The following protected amino acids were then added stepwise: N^{α}-Fmoc-Ile-OH, N^{α}-Fmoc-Arg(Pbf)-OH, N^{α}-Fmoc-Gly OH, N^{α}-Fmoc-Leu-OH, N^{α}-Fmoc-Phe-OH, N^{α}-Fmoc-Lys(Boc)-OH, N^{α}-Fmoc-Ser(tBu)-OH, N^{α}-Fmoc-Phe-OH, N^{α}-Fmoc-Trp(Boc)-OH, N^{α}-Fmoc-Gln(Trt)-OH, N^{α}-Fmoc-Val-OH, and N^{α} -Fmoc-Phe-OH. Each coupling reaction was accomplished using a 3-fold excess of amino acid with HBTU and HOBt in the presence of DIEA.

The N^{α}-Fmoc protecting groups were removed by treating the protected peptide resin with a 25% solution of piperidine in DMF (1 × 5 min and 1 × 20 min). The peptide resin was washed three times with DMF, and the next coupling step was initiated in a stepwise manner. All reactions were performed under an Ar atmosphere. The peptide resin was washed with DCM (3×), DMF (3×), and DCM (4×), and the deprotection protocol was repeated after each coupling step. The N-terminal Fmoc group was removed as described above, and the peptide was released from the resin with TFA/Et_3SiH/H_2O (90:5:5) for 3 h. The resin was removed by filtration, and the crude peptide was recovered by precipitation with cold anhydrous ethyl ether to give a white powder which was purified by RP-HPLC on a semipreparative C18-bonded silica column (Vydac 218TP1010, 1.0 cm × 25 cm) using a gradient of CH_3CN in 0.1% aqueous TFA (from 10% to 90% in 30 min) at a flow rate of 1.0 mL/min. The product was obtained by lyophilization of the appropriate fractions after removal of the CH_3CN by rotary evaporation. Analytical RP-HPLC indicated a purity >98%, and molecular weights were confirmed by MALDI (Kratos Analytical model Kompact). (Table E, Supporting Information).

Microorganisms. The following bacterial strains were used: the Gram-negative *Enterobacter faecalis* ATCC 29212, *Escherichia coli* D21, *Yersinia pseudotuberculosis* YPIII, *Pseudomonas aeruginosa* ATCC 15692, *Pseudomonas syringae* pv tobaci 1918 NCPPB; the Gram-positive *Bacillus megaterium* Bm11, *Staphylococcus aureus* Cowan I, *Staphylococcus aureus* ATCC 25923, *Staphylococcus capitis* n.1, *Staphylococcus epidermidis* ATCC 12228, *Streptococcus pyogenes* ATCC 21547; the yeasts *Candida albicans* ATCC 10231, *Saccharomyces cerevisiae* and *Saccharomyces pombe*.

Antimicrobial Assay. Susceptibility testing was performed by the microbroth dilution method according to the procedures outlined by the National Committee for Clinical Laboratory Standards (2001) using sterile 96-well plates. Aliquots (50 μL) of bacteria in midlog phase at a concentration of 2×10^6 colony-forming units (CFU)/mL in culture medium (Mueller-Hinton, MH) were added to 50 μL of MH broth containing the peptide in serial 2-fold dilutions in 20% ethanol. The ranges of peptide dilutions used were 0.75−24 μM. The same procedure was followed with yeast strains but using Winge medium.[51]

Inhibition of microbial growth was determined by measuring the absorbance at 600 nm after an incubation of 18–20 h at 37 °C (30 °C for yeasts), with a 450-Bio-Rad microplate reader. Antimicrobial activities were expressed as the minimal inhibitory concentration (MIC), the concentration of peptide at which 100% inhibition of microbial growth is observed after 18–20 h of incubation.

Hemolytic Assay. The hemolytic activity was measured on human red blood cells as reported previously.[18] Briefly, aliquots of a human erythrocyte suspension in 0.9% (w/v) NaCl were incubated with serial 2-fold dilutions of peptide (dissolved in 20% ethanol prior to use) for 30 min at 37 °C with gentle mixing. The samples were then centrifuged, and the absorbance of the supernatants was measured at 415 nm. Complete lysis was measured by suspending erythrocytes in distilled water.[19]

Material for Spectroscopic Studies. Samples of 99.9% ^2H_2O were obtained from Aldrich (Milwaukee, WI), and 98% SDS-d_{25} and DPC-d_{38} were obtained from Cambridge Isotope Laboratories, Inc. (Andover, MA). [(2,2,3,3-Tetradeuterio-3-(trimethylsilanyl)]-propionic acid (TSP) was from MSD Isotopes (Montreal, Canada). The 16-doxylstearic acids were from Sigma, and the $MnCl_2$ was from Merck (Darmstadt, Germany).

Circular Dichroism. All CD spectra were recorded using a JASCO J710 spectropolarimeter at 25 °C, with a cell of 1 mm path length. The CD spectra were performed using a measurement range from 260 to 190 nm, 1 nm bandwidth, 4 accumulations, and 100 nm/min scanning speed. CD spectra of TA and TL, at a concentration of 0.1 mM, were performed in water (pH 7.4), in SDS (20 mM), and in DPC (20 mM) micellar solutions.

NMR Spectroscopy. The samples for NMR spectroscopy were prepared by dissolving the appropriate amount of peptide in 0.55 mL of ^1H_2O (pH 4.5), 0.05 mL of ^2H_2O to obtain a concentration of 1–2 mM peptides and 200 mM SDS-d_{25} or DPC-d_{38}. NH exchange studies were performed by dissolving peptides in 0.60 mL of ^2H_2O and 200 mM SDS-d_{25} or DPC-d_{38}. NMR spectra were recorded on a Varian Unity INOVA 700 MHz spectrometer equipped with a z-gradient 5 mm triple-resonance probe head. All the spectra were recorded at a temperature of 298.1 K. The spectra were calibrated relative to TSP (0.00 ppm) as internal standard. One-dimensional (1D) NMR spectra were recorded in the Fourier mode with quadrature detection. 2D DQF-COSY,[39] TOCSY,[40] and NOESY[41] spectra were recorded in the phase-sensitive mode using the method from States.[52] Data block sizes were 2048 addresses in t_2 and 512 equidistant t_1 values. A mixing time of 70 ms was used for the TOCSY experiments. NOESY experiments were run with mixing times in the range of 150–300 ms. The water signal was suppressed by gradient echo.[53] The 2D NMR spectra were processed using the NMRPipe package.[54] Before Fourier transformation, the time domain data matrices were multiplied by shifted $\sin^2$ functions in both dimensions, and the free induction decay size was doubled in F1 and F2 by zero filling.

The qualitative and quantitative analyses of DQF-COSY, TOCSY, and NOESY spectra were obtained using the interactive program package XEASY.[42] The temperature coefficients of the amide proton chemical shifts were calculated from 1D ^1H NMR and 2D TOCSY experiments performed at different temperatures in the range 298–320 K by means of linear regression.

Spin-Label Experiments. The NMR samples were prepared by dissolving 2 mM of peptides in 200 mM deuterated SDS solution in H_2O/D_2O 90:10. Assuming an SDS micelle aggregation number of 56, this corresponds to a micelle concentration of 3.6 mM. The 16- doxylstearic acids (solubilized in DMSO-d_6) and Mn^{2+} (dissolved in H_2O) were added to the samples at a concentration of one spin label per micelle.

Structural Determinations and Computational Modeling. The NOE-based distance restraints were obtained from NOESY spectra collected with a mixing time of 200 ms. The NOE cross peaks were integrated with the XEASY program and were converted into upper distance bounds using the CALIBA program incorporated into the program package DYANA.[44] Only NOE derived constraints (Supporting Information) were considered in the annealing procedures. An error tolerant target function (tf type 3) was used to account for the peptide intrinsic flexibility. For each examined peptide, an ensemble of 200 structures was generated with the simulated annealing of the program DYANA. Then 100/200 structures were chosen, whose interprotonic distances best fitted NOE derived distances, and refined through successive steps of restrained and unrestrained EM calculations using the Discover algorithm (Accelrys, San Diego, CA) and the consistent valence force field (CVFF).[55] The minimization lowered the total energy of the structures; no residue was found in the disallowed region of the Ramachandran plot. The final structures were analyzed using the InsightII program (Accelrys, San Diego, CA). Graphical representation were carried out with the InsightII program (Accelrys, San Diego, CA). The root-mean-squared-deviation analysis between energy-minimized structures were carried out with the program MOLMOL.[56] The PROMOTIF program was used to extract details on the location and types of structural secondary motifs.[57]

Supporting Information Available: NMR data of the analyzed peptides and physicochemical data of the TA, TL, and new analogues. This material is available free of charge via the Internet at http://pubs.acs.org.

References

(1) Boman, H. G. Innate immunity and the normal microflora. *Immunol Rev.* **2000**, *173*, 5–16.
(2) Zasloff, M. Antimicrobial peptides of multicellular organisms. *Nature* **2002**, *415*, 389–395.
(3) Mangoni, M. L.; Miele, R.; Renda, T. G.; Barra, D.; Simmaco, M. The synthesis of antimicrobial peptides in the skin of *Rana esculenta* is stimulated by microorganisms. *FASEB J.* **2001**, *15*, 1431–1432.
(4) Bulet, P.; Stocklin, R.; Menin, L. Anti-microbial peptides: from invertebrates to vertebrates. *Immunol. Rev.* **2004**, *198*, 169–184.
(5) Zaiou, M. Multifunctional antimicrobial peptides: therapeutic targets in several human diseases. *J. Mol. Med.* **2007**, *85*, 317–329.
(6) Boman, H. G. Peptide antibiotics and their role in innate immunity. *Annu. Rev. Immunol.* **1995**, *13*, 61–92.
(7) Boman, H. G. Antibacterial peptides: basic facts and emerging concepts. *J. Intern. Med.* **2003**, *254*, 197–215.
(8) Kimbrell, D. A.; Beutler, B. The evolution and genetics of innate immunity. *Nat. Rev. Genet.* **2001**, *2*, 256–267.
(9) Hancock, R. E. W. Cationic peptides: effectors in innate immunity and novel antimicrobials. *Lancet Infect. Dis.* **2001**, *1*, 156–164.
(10) Mookherjee, N.; Hancock, R. E. Cationic host defence peptides: innate immune regulatory peptides as a novel approach for treating infections. *Cell. Mol. Life Sci.* **2007**, *64*, 922–933.
(11) Papagianni, M. Ribosomally synthesized peptides with antimicrobial properties: biosynthesis, structure, function, and applications. *Biotechnol. Adv.* **2003**, *21*, 465–499.
(12) Rinaldi, A. C. Antimicrobial peptides from amphibian skin: an expanding scenario. *Curr. Opin. Chem. Biol.* **2002**, *6*, 799–804.
(13) Simmaco, M.; Mignogna, G.; Canofeni, S.; Miele, R.; Mangoni, M. L.; Barra, D. Temporins, antimicrobial peptides from the European red frog *Rana temporaria*. *Eur. J. Biochem.* **1996**, *242*, 788–792.
(14) Wade, D.; Silberring, J.; Soliymani, R.; Heikkinen, S.; Kilpeläinen, I.; Lankinen, H.; Kuusela, P. Antibacterial activities of temporin A analogs. *FEBS Lett.* **2000**, *479*, 6–9.

(15) Wade, D.; Silveira, A.; Silberring, J.; Kuusela, P.; Lankinen, H. Antibiotic properties of novel synthetic temporin A analogs and a cecropin A-temporin A hybrid peptide. *Protein Pept. Lett.* **2000**, *7*, 349–357.
(16) Wade, D. Unambiguous consensus sequences for temporin-like antibiotic peptides. *Internet J. Chem.* **2002**, *5*, 5. [Online, http://preprint.chemweb.com/biochem/0204002].
(17) Mangoni, M. L. Temporins, anti-infective peptides with expanding properties. *Cell. Mol. Life Sci.* **2006**, *63*, 1060–1069.
(18) Rinaldi, A. C.; Mangoni, M. L.; Rufo, A.; Luzi, C.; Barra, D.; Zhao, H.; Kinnunen, P. K. J.; Bozzi, A.; Di Giulio, A.; Simmaco, M. Temporin L: antimicrobial, hemolytic and cytotoxic activities, and effects on membrane permeabilization in lipid vesicles. *Biochem. J.* **2002**, *368*, 91–100.
(19) Mangoni, M. L.; Rinaldi, A. C.; Di Giulio, A.; Mignogna, G.; Bozzi, A.; Barra, D.; Simmaco, M. Structure−function relationships of temporins, small antimicrobial peptides from amphibian skin. *Eur. J. Biochem.* **2000**, *267*, 1447–1454.
(20) Rinaldi, A. C.; Di Giulio, A.; Liberi, M.; Gualtieri, G.; Oratore, A.; Schinina, M. E.; Simmaco, M.; Bozzi, A. Effects of temporins on molecular dynamics and membrane permeabilization in lipid vesicles. *J. Pept. Res* **2001**, *58*, 213–220.
(21) Zhao, H.; Rinaldi, A. C.; Di Giulio, A.; Simmaco, M.; Kinnunen, P. K. J. Interactions of the antimicrobial peptides temporins with model biomembranes. Comparison of temporins B and L. *Biochemistry* **2002**, *41*, 4425–4436.
(22) Mangoni, M. L.; Saugar, J. M.; Dellisanti, M.; Barra, D.; Simmaco, M.; Rivas, L. Temporins, small antimicrobial peptides with leishmanicidal activity. *J. Biol. Chem.* **2005**, *280*, 984–990.
(23) Mangoni, M. L.; Papo, N.; Barra, D.; Simmaco, M.; Bozzi, A.; Di Giulio, A.; Rinaldi, A. C. Effects of the antimicrobial peptide temporin L on cell morphology, membrane permeability and viability of *Escherichia coli*. *Biochem. J.* **2004**, *380*, 859–865.
(24) Shai, Y. Mechanism of the binding, insertion and destabilization of phospholipid bilayer membranes by alpha-helical antimicrobial and cell non-selective membrane-lytic peptides. *Biochim. Biophys. Acta* **1999**, *1462*, 55–70.
(25) Matsuzaki, K. Why and how are peptide−lipid interactions utilized for self-defense? Magainins and tachyplesins as archetypes. *Biochim. Biophys. Acta* **1999**, *1462*, 1–10.
(26) Yang, L.; Weiss, T. M.; Lehrer, R. I.; Huang, H. W. Crystallization of antimicrobial pores in membranes: magainin and protegrin. *Biophys. J.* **2000**, *79*, 2002–2009.
(27) Gidalevitz, D.; Ishitsuka, Y.; Muresan, A. S.; Konovalov, O.; Waring, A. J.; Lehrer, R. I.; Lee, K. Y. Interaction of antimicrobial peptide protegrin with biomembranes. *Proc. Natl. Acad. Sci. U.S.A.* **2003**, *100*, 6302–6307.
(28) Yeaman, M. R.; Yount, N. Y. Mechanisms of antimicrobial peptide action and resistance. *Pharmacol. Rev.* **2003**, *55*, 27–55.
(29) Langham, A. A.; Khandelia, H.; Kaznessis, Y. N. How can a β-sheet peptide be both a potent antimicrobial and harmfully toxic? Molecular dynamics simulations of protegrin-1 in micelles. *Biopolymers* **2006**, *84*, 219–231.
(30) Henry, G. D.; Sykes, B. D. Methods to study membrane protein structure in solution. *Methods Enzymol.* **1994**, *239*, 515–535.
(31) Kallick, D. A.; Tessmer, M. R.; Watts, C. R.; Li, C. Y. J. The use of dodecylphosphocholine micelles in solution NMR. *J. Magn. Reson. B* **1995**, *109*, 60–65.
(32) Lee, S. A.; Kim, Y. K.; Lim, S. S.; Zhu, W. L.; Ko, H.; Shin, S. Y.; Hahm, K. S.; Kim, Y. Solution structure and cell selectivity of piscidin 1 and its analogues. *Biochemistry* **2007**, *46*, 3653–3663.
(33) van den Hooven, H. W. S.; Chris, A. E. M.; van de Kamp, M.; Konings, R. N. H.; Hilbers, C. W.; van de Ven, F. J. M. Three-dimensional structure of the lantibiotic nisin in the presence of membrane-mimetic micelles of dodecylphosphocholine and of sodium dodecylsulphate. *Eur. J. Biochem.* **1996**, *235*, 394–403.
(34) Atherton, E.; Sheppard, R. C. *Solid-Phase Peptide Synthesis: A Practical Approach*; IRL Press: Oxford, U.K., 1989.
(35) D'Abramo, M.; Rinaldi, A. C.; Bozzi, A.; Amadei, A.; Mignogna, G.; Di Nola, A.; Aschi, M. Conformational behavior of temporin A and temporin L in aqueous solution: a computational/experimental study. *Biopolymers* **2006**, *81*, 215–224.
(36) Kamysz, W.; Mickiewicz, B.; Rodziewicz-Motowidlo, S.; Greber, K.; Okroj, M. Temporin A and its retro-analogues: synthesis, conformational analysis and antimicrobial activities. *J. Pept. Sci.* **2006**, *12*, 533–537.
(37) Zhao, H; Kinnunen, P. K. Binding of the antimicrobial peptide temporin L to liposomes assessed by Trp fluorescence. *J. Biol. Chem.* **2002**, *277*, 25170–25177.
(38) Wüthrich, K. In *NMR of Proteins and Nucleic Acids*; John Wiley & Sons, Inc.: New York, 1986.
(39) (a) Piantini, U.; Sorensen, O. W.; Ernst, R. R. Multiple quantum filters for elucidating NMR coupling network. *J. Am. Chem. Soc.* **1982**, *104*, 6800–6801. (b) Marion, D.; Wüthrich, K. Application of phase sensitive two-dimensional correlated spectroscopy (COSY) for measurements of $^1H-^1H$ spin−spin coupling constants in proteins. *Biochem. Biophys. Res. Commun.* **1983**, *113*, 967–974.
(40) Braunschweiler, L.; Ernst, R. R. Coherence transfer by isotropic mixing: application to proton correlation spectroscopy. *J. Magn. Reson.* **1983**, *53*, 521–528.
(41) Jenner, J.; Meyer, B. H.; Bachman, P.; Ernst, R. R. Investigation of exchange processes by two-dimensional NMR spectroscopy. *J. Chem. Phys.* **1979**, *71*, 4546–4553.
(42) Bartels, C.; Xia, T.; Billeter, M.; Guentert, P.; Wüthrich, K. The program XEASY for computer-supported NMR spectral analysis of biological macromolecules. *J. Biomol. NMR* **1995**, *6*, 1–10.
(43) (a) Wishart, D. S.; Sykes, B. D.; Richards, F. M. The chemical shift index: a fast method for the assignment of protein secondary structure through NMR spectroscopy. *Biochemistry* **1992**, *31*, 1647–1651. (b) Andersen, N. H.; Liu, Z.; Prickett, K. S. Efforts toward deriving the CD spectrum of a 3(10) helix in aqueous medium. *FEBS Lett.* **1996**, *399*, 47–52.
(44) Güntert, P.; Mumenthaler, C.; Wüthrich, K. Torsion angle dynamics for NMR structure calculation with the new program DYANA. *J. Mol. Biol.* **1997**, *273*, 283–298.
(45) (a) Brown, L. R.; Bösch, C.; Wüthrich, K. Location and orientation relative to the micelle surface for glucagon in mixed micelles with dodecylphosphocholine: EPR and NMR studies. *Biochim. Biophys. Acta* **1981**, *642*, 296–312. (b) Lindberg, M.; Jarvet, J.; Langel, U.; Graslund, A. Secondary structure and position of the cell-penetrating peptide transportan in SDS micelles as determined by NMR. *Biochemistry* **2001**, *40*, 3141–3149.
(46) Shai, Y. Molecular recognition between membrane-spanning polypeptides. *Trends Biochem. Sci.* **1995**, *20*, 460–464.
(47) Matsuzaki, K. Magainins as paradigm for the mode of action of pore forming polypeptides. *Biochim. Biophys. Acta* **1998**, *1376*, 391–400.
(48) Wu, M.; Maier, E.; Benz, R.; Hancock, R. E. W. Mechanism of interaction of different classes of cationic antimicrobial peptides with planar bilayers and with the cytoplasmic membrane of *Escherichia coli*. *Biochemistry* **1999**, *38*, 7235–7242.
(49) Wieprecht, T.; Dathe, M.; Epand, R. M.; Beyermann, M.; Krause, E.; Maloy, W. L.; MacDonald, D. L.; Bienert, M. Peptide hydrophobicity controls the activity and selectivity of magainin 2 amide in interaction with membranes. *Biochemistry* **1997**, *36*, 6124–6132.
(50) Sharon, M.; Oren, Z.; Shai, Y.; Anglister, J. 2D-NMR and ATR-FTIR study of the structure of a cell-selective diastereomer of melittin and its orientation in phospholipids. *Biochemistry* **1999**, *38*, 15305–15316.
(51) Valenti, P.; Visca, P.; Antonini, G.; Orsi, N. Antifungal activity of ovotransferrin towards genus *Candida*. *Mycopathologia* **1985**, *89*, 169–175.
(52) States, D. J.; Haberkorn, R. A.; Ruben, D. J. A two-dimensional nuclear Overhauser experiment with pure absorption phase in four quadrants. *J. Magn. Reson.* **1982**, *48*, 286–292.
(53) Hwang, T. L.; Shaka, A. J. Water suppression that works. Excitation sculpting using arbitrary wave-forms and pulsed-field gradients. *J. Magn. Reson.* **1995**, *112*, 275–279.
(54) Delaglio, F.; Grzesiek, S.; Vuister, G. W.; Zhu, G.; Pfeifer, J.; Bax, A. NMRPipe: a multidimensional spectral processing system based on UNIX pipes. *J. Biomol. NMR* **1995**, *6*, 277–93.
(55) Maple, J.; Dinur, U.; Hagler, A. T. Derivation of force fields for molecular mechanics and dynamics from ab initio energy surface. *Proc. Natl. Acad. Sci. U.S.A.* **1988**, *85*, 5350–5354.
(56) Koradi, R.; Billeter, M.; Wüthrich, K. MOLMOL: a program for display and analysis of macromolecular structures. *J. Mol. Graphics* **1996**, *14*, 51–55.
(57) Hutchinson, E. G.; Thornton, J. M. PROMOTIF—a program to identify and analyze structural motifs in proteins. *Protein Sci.* **1996**, *5*, 212–220.

JM701604T